Chapter 12

Determination of the Road Surface Microtexture

12.1 Introduction

12.1.1 Context: road safety field

If our vehicles are always safer as the mechanics, the electronics and the computer science progress, it is also mandatory, in the road safety field, to investigate the road surface quality.

The latter can particularly be characterized by the *skid resistance*, i.e. the property of the trafficked surface to maintain the adhesion of a vehicle tire, or the *friction*, stating the resistance to relative motion between the tire and the road [57]. A recent study [58] made by the Belgian Road Research Center (BRRC) tends to show that these parameters could be deduced from both the road surface micro– and macrotexture. Distinction between both textures lays on the wavelength, i.e. spatial period: the respective span is 50 μm – 500 μm and 0.5 mm – 50 mm for micro– and macrotexture [59].

Microtexture varies from harsh, when the road is newly constructed, to polished, under the effects of traffic and weather conditions.

Surface texture, measured at the micron scale of harshness, is known to be a function of the mineralogy and petrology of the aggregate particles. Under this heading comes also the texture of bituminous and cement mortars, which may occupy major portions of the asphalt surface between any exposed coarse aggregate particles.

Generally speaking, microtexture affects the *skid resistance* of the road surface, at all speeds. Under wet conditions, it breaks the water film in the tire/road contact area, explaining why surfaces with sharp microtexture have a high wet skid resistance at low speed (the side effect being that they are associated with a high rate of tire wear). But without macrotexture, they exhibit a steep decline in friction as speed rises. This shows why both macro– and microtexture are important for the determination of the skid resistance.

Automated instruments actually exist, allowing the in-situ determination of the road macrotexture only. The vast majority uses laser triangulation, but in some cases structured lighting is involved [60].

Concerning microtexture, there is a clear lack of available instruments, which explains the initiation of this study by our laboratory. This chapter presents its developments, results and conclusions.

12.1.2 Positioning of the problem

By *in-situ determination of the road microtexture*, one means the determination of the road surface vertical microprofile, the instrument being e.g. attached on a moving vehicle and taking real-time measurements. It is to be noted that contrarily to the previous applications presented in this work, one has no prior knowledge about the shape of the sample under study. The present application remains however in the scope of the thesis since laser plane lighting is involved, and the aim is still to be able to operate in an ambulatory environment.

Once the microprofile is determined, further mathematical and statistical treatments—still under investigation at the BRRC—associated with macrotexture information, will allow the user to determine the *skid resistance* (see for instance [61]).

As a first step, in order to simplify the problem, we focus on laboratory-made microprofile measurements on samples immobile regarding the instrument.

The performances to be achieved by our instrument are a combination of recommendations coming from the ISO13473-3:2002 international standard [62], dealing with optical profilometers of road surfaces, and demands of the BRRC. They are listed on Table 12.1 (the right column is reserved for later). To summarize, the microprofile must thus be established at a distance and without contact, on a 2-mm width, for amplitudes going up to 2 mm. The longitudinal sampling interval must be of 20 ± 2 μm. The needed resolutions in the vertical direction is of 1 μm, and the required accuracy in the same direction is of 40 μm.

Table 12.1. Performances of Optical Profilometers of Road Surfaces

quantity	microtexture	macrotexture
texture wavelengths	50–500 μm	0.5–200 mm
horizontal length of the profile	2 mm	500 mm
horizontal sampling interval	20 ± 2 μm	200 ± 20 μm
vertical range	2 mm	20 mm
vertical resolution	1 μm	10μm
vertical accuracy	40 μm	400 μm

12.1.3 Organization

This chapter is organized in an intuitive way. At first, the instrument is presented in Section 12.2.

Right after, we present the method used for the vertical road profile determination (Section 12.3). Section 12.4 details the dimensioning of the pre-prototype.

After a short description of the image processing algorithm (Section 12.5), we illustrate how we dealt with speckle in Section 12.6.

In Section 12.7, we calculate the error that one can expect on the microprofiles, using the accuracy analysis of Chapter 7.

Some considerations are then given about the instrument calibration (Section 12.8). The next step is the validation of the pre-prototype on calibrated microprofiles, detailed in Section 12.9, and we then explain what would have occurred if our theoretical models were not so complete (Section 12.10).

After having presented the ambulatory instrument, developed for the combined measurement of the micro– and macrotexture of road surfaces (12.11), we show some results obtained on a real road surface (Section 12.12). Some conclusions close this chapter.

Note that the present chapter groups and develops two papers previously published [63] [64].

12.2 Description of the Instrument

The instrument used is conceptually sensibly the same as that described in Section 9.4, even though—as it will be detailed in section 12.4—the hardware used is completely different.

The road sample, supposed horizontal, is illuminated by a vertical laser plane, which creates a curve on the sample.

The scene is observed by a monochrome CCD camera slightly tilted on the vertical direction (see Fig. 12.1). Systems of reference (x, y, and z) and (x_{pix}, y_{pix}) are as defined in Chapter 2.

The surface of the target is supposed at least partially diffusing, so that in any case, the camera receives a part of the laser plane luminance reflected by the sample.

Contrarily to all the other applications presented in this work, it was not necessary to place a narrow-band interference filter between the CCD sensor of the camera and its objective. As detailed in Section 12.4, to achieve the resolutions required for this particular application, a camera lens of high focal length was needed, with the consequence that the entire scene—the laser plane excepted—was almost invisible to the camera sensor.

Our instrument is defined by ten parameters: seven for the camera (see Chapter 2) and three for the laser plane (see Fig. 12.2, where ϵ is not represented and Section 3.4). We will however see in Section 12.4 that some of the camera imperfections can be neglected.

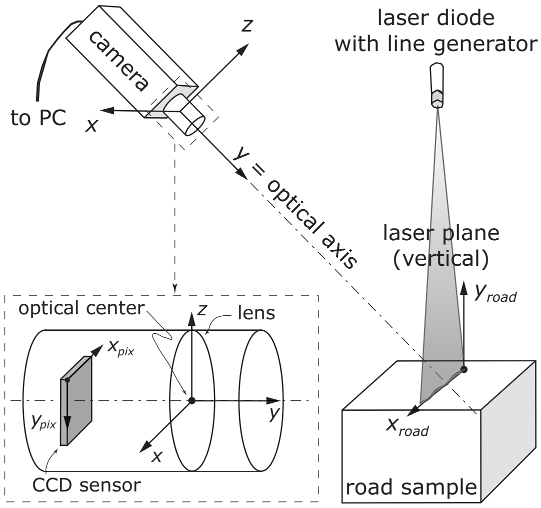

Fig. 12.1. Configuration of the device. 3-D view.

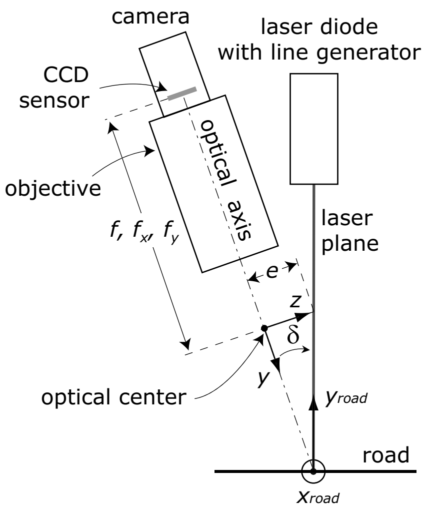

Fig. 12.2. Geometry of the device. Cut in the vertical plane (y, z).

12.3 Determination of the Vertical Road Profile

As shown in Chapter 3, a one-to-one correspondence exists between the ICS coordinates of any pixel of the laser curve and the WCS coordinates of the corresponding point in the scene.

We can thus assess that the coordinates of every point of the laser curve are known in the WCS by (3.7).

It allows us to determine the vertical road profile (x_{road}, y_{road}) by mean of a simple coordinate transformation (x_{road} is the horizontal direction aligned with the laser plane, y_{road} is the vertical direction; see Fig. 12.1):

$$\begin{cases} x_{road} & = & x\cos\epsilon + y\sin\epsilon \\ y_{road} & = & -y\cos\delta + z\sin\delta \end{cases} \tag{12.1}$$

It is not necessary to make a translation of the coordinate system from the optical center to the road as the profile is defined by amplitude variations around a central value.

Note that the need to define a new coordinate system different from that of the camera is also known as *localization* [8]. This concept usually requires the introduction of six *extrinsic* camera parameters (three for the rotation and three for the translation). It is not developed here since (a) no translation is required and (b) only two rotations are enough, by angles that happen to be δ and ϵ, also defining the laser plane orientation.

12.4 Pre-prototype

We use an industrial monochrome CCD camera, the sensor of which is composed of 576x768 square pixels, with 1/160-mm side (the smallest sensor side being in the x_{pix} direction; see "Camera #2" on TABLE 4.1).

The camera lens has a field of view of 2 mm in the x direction (i.e. also in x_{road} direction in first approximation, as ϵ is close to zero) at the optimal working distance D—between the optical center and the road—of about 100 mm. Its focal length f is of approximatively 200 mm (see "Lens #2" on TABLE 4.2). It offers the advantage to present a negligible radial distortion (smaller than 0.15%, guaranteed by the manufacturer).

This configuration ensures a satisfactory longitudinal resolution of $2/576$ mm $= 3.5\ \mu$m.

In the transversal direction, the resolution is virtually infinitely small: the center of the laser curve is determined with subpixel resolution, as detailed in Section 5.7.1.

Anticipating the fact that we will have to deal with speckle in this application, we can assess (see Section 5.7.2) that the maximum error on the center location of the laser curve is of ± 1 pixel.

This will cause an absolute error on the altitude Δy_{road} of (see Section 7.2):

$$\Delta y_{road} = \frac{D\sqrt{D^2 + e^2}}{ef} \tag{12.2}$$

which, from Table 12.1, has to be smaller than 40 μm. This implies that distance e must be at least 8 mm. Angle δ will be fixed so that the laser curve remains in the field of view of the camera in any situation.

The laser plane generator we use offers a 16-μm-thick line at the optimal working distance (of the order of 25 cm; see "Laser #3" on Table 4.3).

Fig. 12.3 shows a photograph of the instrument.

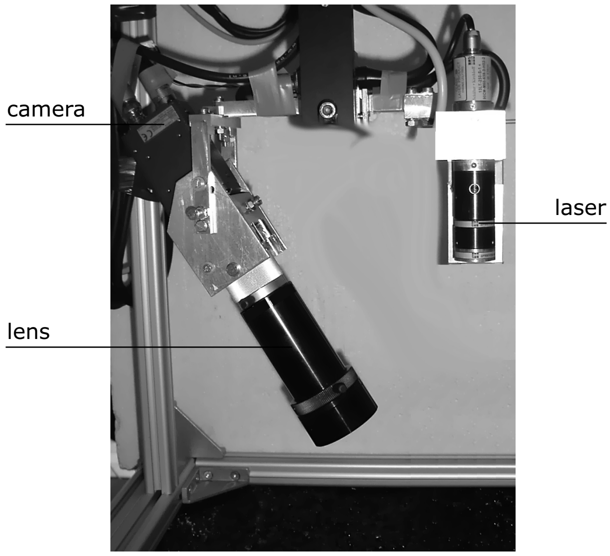

Fig. 12.3. Photograph of the instrument.

12.5 Image Processing

An image processing algorithm extracts the laser curve intersected by the road surface by isolating it from the rest of the scene.

The treatments to perform on the image are (see Chapter 5 for a description of each item):

- subtraction of two pictures sequentially taken (one with the laser diode on, the other with the diode off);
- thresholding;
- segmentation;
- laser curve selection;
- speckle Gaussian 2-D FIR low-pass filtering;
- column-by-column subpixel location of the curve.

Note that the correction of the lens distortion does not appear in this list. This will be justified in Section 12.8.

The output of this algorithm consists of a list containing the coordinates in the ICS of all the pixels belonging to the laser curve.

12.6 Dealing with Speckle

At the working distance D of the camera, our device is subject to the major problem of laser speckle (see Section 7.3).

This phenomenon could induce a disqualifying limitation to the accuracy achievable by the instrument and has thus to be eliminated at best.

The first measure taken is to open the camera's diaphragm at its maximum. It decreases the size of each speckle, as shown in (7.9). It has the disadvantage of diminishing the depth of field of the camera, but without any incidence in our case.

The second action against speckle is the digital filtering suggested in Section 5.7.2.

Fig. 12.4 sequentially shows the effect of both precautions on a typical acquired image.

12.7 Expected Accuracy

Contrarily to the other applications, it is here rather easy to proceed to an analytical study of the vertical accuracy that one can expect on the microprofiles, in a similar way than in Chapter 7.

The expression of the error must take into account the fact that every ordinate y_{road} of the microprofile is referred to a "reference" altitude $y_{road,ref}$, e.g. obtained by considering the central ordinate in the image. Some error

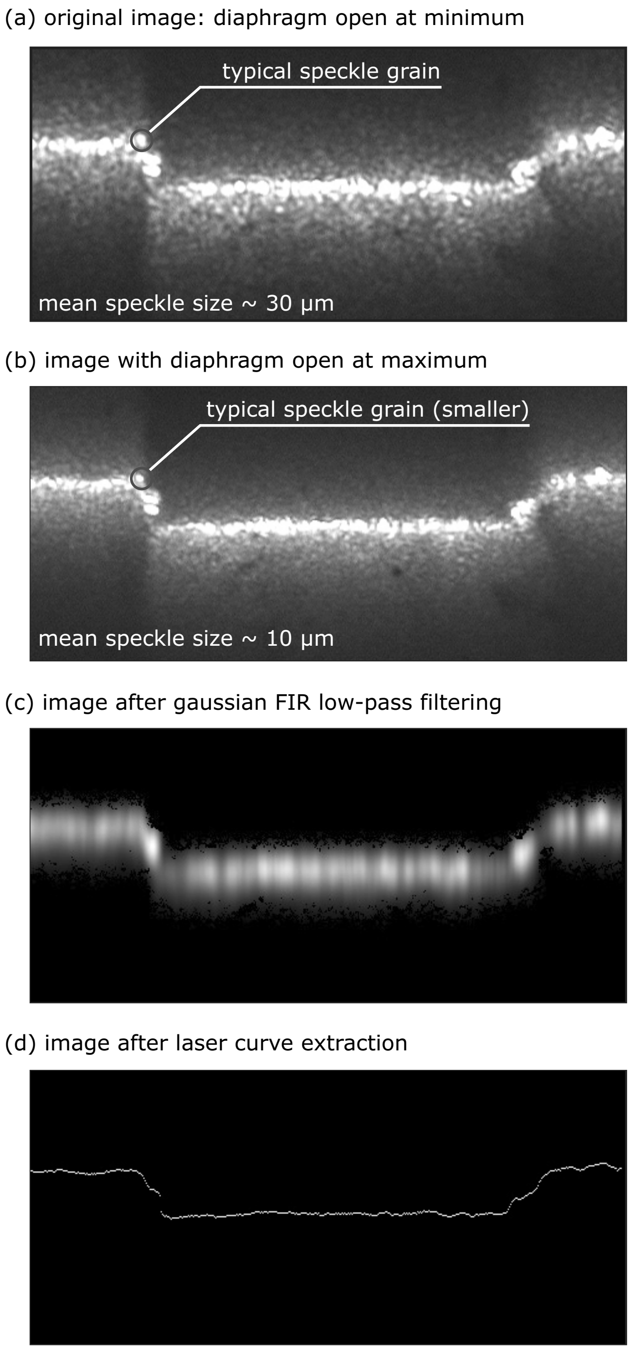

Fig. 12.4. Dealing with speckle.

terms in y_{road} and $y_{road,ref}$ will thus be common and compensate each other. It would therefore be erroneous to calculate the errors separately.

From (12.1) and (7.1)—i.e. we make the same suppositions than in Chapter 7 regarding γ and ϵ—the expression on which we have to work is:

$$y_{road} - y_{road,ref} = \frac{e f_x \left(y_{pix} - y_{pix,ref}\right)}{\cos\delta \left(y_{pix} + f_x \tan\delta\right)\left(y_{pix,ref} + f_x \tan\delta\right)} \tag{12.3}$$

where y_{pix} and $y_{pix,ref}$ are the ICS ordinates of (respectively) the "unknown" and reference points. It is important to note that $y_{pix,ref}$ serves only as a common reference for all the points of the microprofile, with the consequence that its location error is nil.

The absolute error $\Delta\left(y_{road} - y_{road,ref}\right)$ on the altitude, abbreviated Δ, can be estimated by using the partial derivatives of this error with regard to the different parameters:

$$\Delta = \left|\frac{\partial\Delta}{\partial y_{pix}}\Delta y_{pix}\right| + \left|\frac{\partial\Delta}{\partial e}e\rho_e\right| + \left|\frac{\partial\Delta}{\partial f_x}f_x\rho_{f_x}\right| + \left|\frac{\partial\Delta}{\partial\delta}\delta\rho_\delta\right| \tag{12.4}$$

where the values of all the parameters and uncertainties are as defined in Chapter 7 (case 2).

Without entering into the analytical details allowing to solve (12.4), we can announce that a total absolute error Δ of 10 μm is obtained, for $y_{road} - y_{road,ref} = \pm 1$ mm (i.e. at the extremes of the required vertical range) and $y = 10$ cm (working distance of the camera). The major contributions come from the errors on y_{pix} (7.6 μm) and on f_x (1.6 μm).

One can thus conclude that the hoped accuracy of 40 μm in the vertical direction can easily be reached—especially seen that this figure of 10 μm has been obtained by considering the worst of the cases, i.e. when the errors terms have their maximum values and the same sign. This will actually be corroborated in the next sections.

12.8 Calibration of the Instrument

Contrarily to the other applications presented in this thesis, the calibration of the instrument could not be divided in two distinct procedures for the camera parameters on one side, and for the laser plane ones on the other. This is due to the fact that it is not possible to print—at reasonable cost—a checker pattern of 2x2 mm (i.e. the camera field of view), and thus to calibrate the camera independently from the laser plane.

It is nevertheless pertinent to admit some simplifications on the camera model for this particular application. Actually, seen the high quality of the camera lens, radial distortion (smaller than 0.15%) and skewness can be neglected. This allows us to eliminate three camera parameters: distortion coefficients k_1 and k_2 and skewness factor γ. (This explains why the correction of the lens distortion is not applied in the image processing stage.)

The remaining parameters constitute the parameter vector $U=(f_x,\ f_y,\ X_{pix,0},\ Y_{pix,0},\ e,\ \delta,\ \epsilon)$ to optimize by mean of the gradient descent method detailed in Section 6.3.

The method now being set, we still need to choose one or more objects to perform the calibration on. Road samples are not suitable since their profiles are a priori not known. Calibrated microprofiles are usually very expensive, and unadapted to our method because not sufficiently diffusing.

The retained solution was to use a voltage-controlled calibrated piezoelectric actuator making vertical movements ranging from 0 to 520 μm. A piece of white paper was pasted on the top plane of the motor (cf. Fig. 12.5). A look-up table of the voltage versus the altitude was used as reference in the gradient descent method, which provided us with the parameter values. We found: $f_x = f_y =$ 30536 pixels (i.e. approximatively 191 mm); $X_{pix,0} = 287.5$ pixels; $Y_{pix,0} =$ 383.5 pixels; $e = 46$ mm; $\delta = 28°$; $\epsilon = 0.2°$. These results are coherent with the camera and lens specifications, and the geometrical configuration of the instrument.

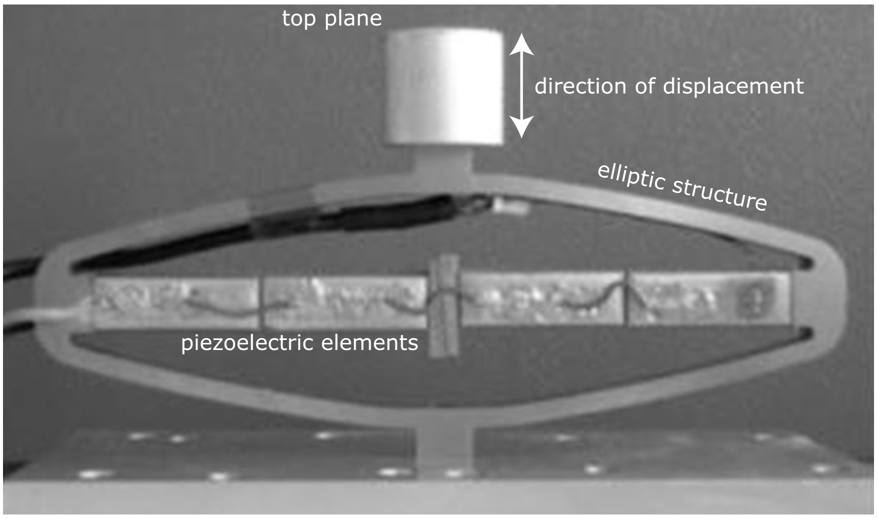

Fig. 12.5. Photograph of the voltage-controlled calibrated piezoelectric actuator. The piezoelectric elements are horizontally placed on the largest axis of the actuator's elliptic structure. The laser plane is projected on the upper basis of the white cylinder at the top of the motor.

The results of the calibration are on Fig. 12.6, comparing the reference altitude and the calibrated one. The absolute error on the measurement remains below 5 μm in any case, with a standard deviation of 1.6 μm. These figures are of course excellent, but were predictable by the accuracy analysis of Section 12.7.

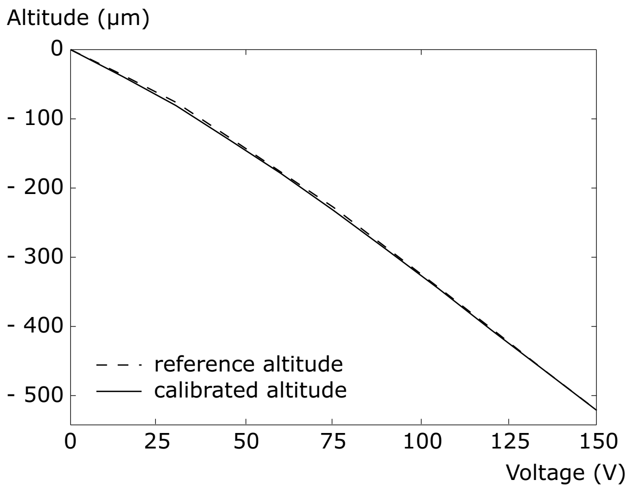

Fig. 12.6. Graph of the altitude of the piezoelectric actuator versus the applied voltage. The reference altitude is in dashed stroke and the measured altitude after calibration in plain stroke. One sees the excellent correspondence between the two curves.

12.9 Validation of the Method

The next step of the study was the validation of the method. To achieve that, we asked the Mechanical Department of our university to manufacture a parallelepipedic piece made of plastic—thus diffusing—material and composed of seven 1-mm-wide furrows of various, known depths going from about 50 μm to about 1 mm (see Fig. 12.7 showing the piece and a close-up on one of the furrows). Note that the actual depths were measured with a stylus profilometer, the accuracy of which was of $\pm 1\mu$m.

The profiles we obtained for two of the furrows are presented on Fig. 12.8 and Fig. 12.9. The *real mean profile* presented on these figures is placed so that (a) its real width and height are respected and (b) the mean squared difference between the real profile and the measured one is minimized. The results are similar for the other five furrows.

The measured profiles permit us to make the following observations:

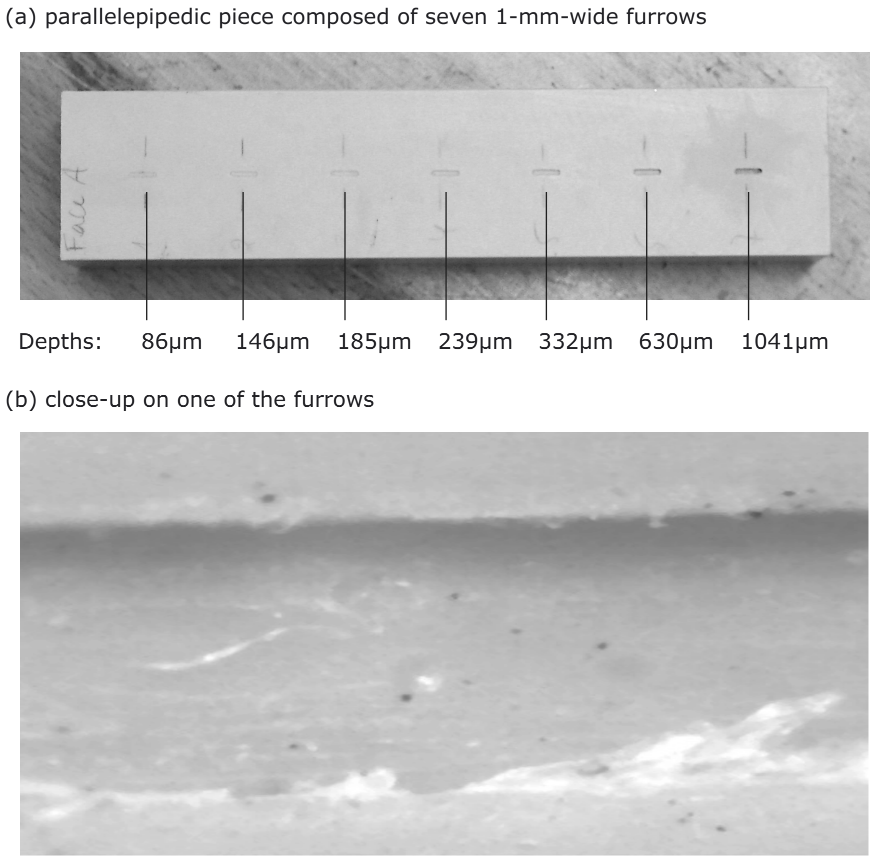

Fig. 12.7. Photographs of (a) the whole parallelepipedic piece and (b) a close-up on one of the furrows.

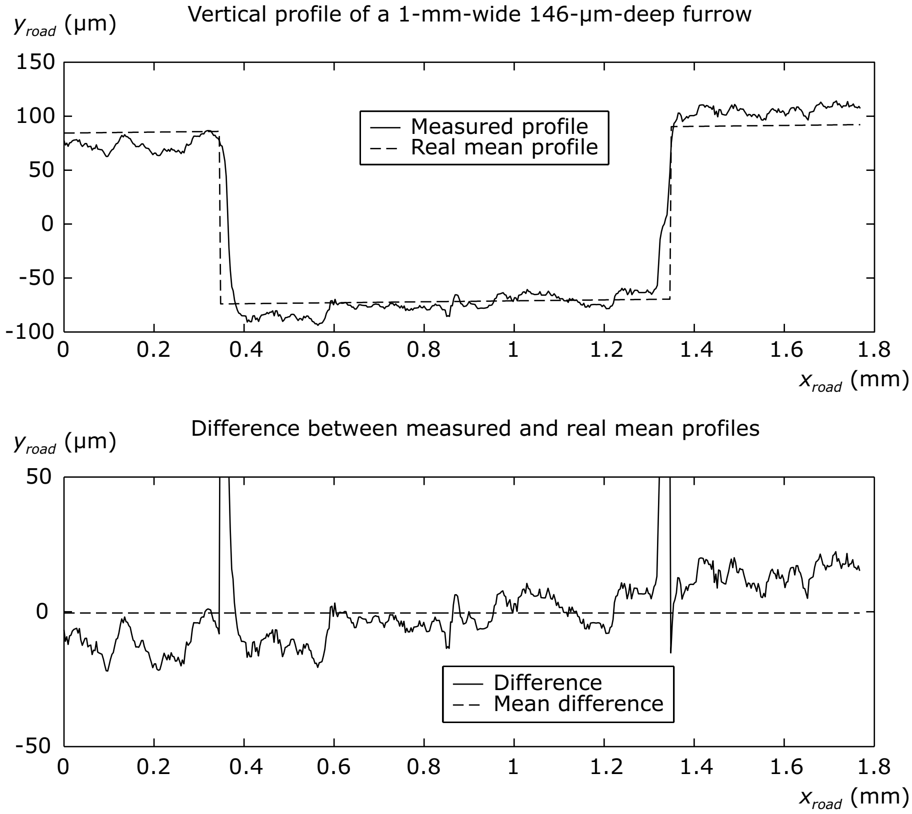

Fig. 12.8. Validation on a 1-mm-wide 146-μm-deep furrow. Comparison between measured and real mean profiles.

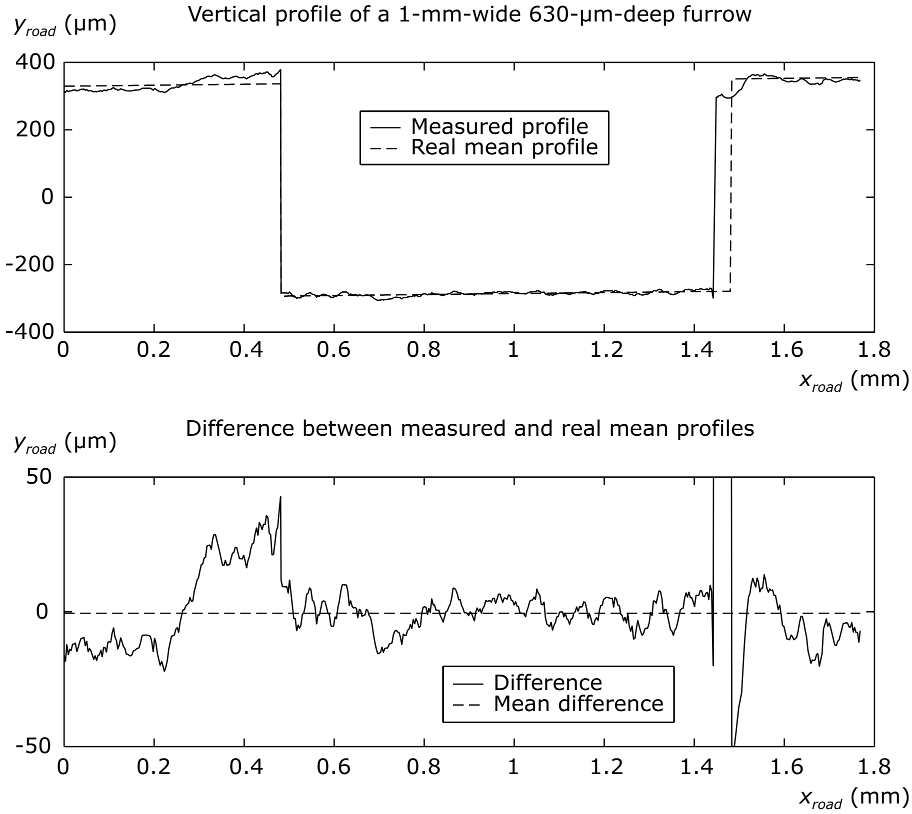

Fig. 12.9. Validation on a 1-mm-wide 630-μm-deep furrow. Comparison between measured and real mean profiles.

- the mean absolute error on the depths is inferior to 5 μm;
- its standard deviation is of about 3 μm;
- the mean rugosity of the profiles observed by our instrument corresponds to that estimated with a vision machine, i.e. 20 μm peak-to-peak;
- the width of the profiles is globally well estimated, but flaws at the edges of the furrows make the estimation difficult. To convince ourselves of the quality of the profile in the x_{road} direction, let us start from the observation that by (12.1) and seen the very low value of ϵ, $x_{road} \cong x$. From the camera model [see (2.3)], and because y is obviously accurate by (12.1), we see that x_{road} is the x_{pix} scale multiplied by an accurate factor y/f_x. We can thus assert that it is of the same relative accuracy as y_{road}, i.e. approximatively 0.005% (5 μm divided by the working distance $D = 100$ mm). It gives a maximum absolute error of a fraction of μm (when $x_{road} = \pm 1$ mm, i.e. at the extremes of the microprofiles).

Those excellent (and predictable) results make us claim that the requirements of TABLE 12.1 are fulfilled.

12.10 Without a Refined Theory...

Since the pre-prototype used in the present chapter is totally different from the one used in the three previous applications, the observations regarding what would have happened if our theoretical models were not so refined are sensibly different:

- Chapter 2: we use a simple camera model, with no distortion, because the quality of the optics allows us to do so. We nevertheless showed that a complete model was necessary for the first three applications;
- Chapters 3 and 6: the same remarks than in Section 9.13 apply;
- Chapter 5: regarding image processing, one can point out (beside all the essential operations allowing to extract the laser curves) that without subpixel location, the error would have been drastically higher (probably multiplied by 3, which was shown as the improvement ratio provided by the algorithm; see Section 5.7.1). Curve smoothing must be avoided imperatively, since it would completely change the microprofile's aspect. But of course, it is the speckle filtering which is the most essential in this application. Without it, the performances would be dramatically degraded (see Section 5.7.2);

These remarks lead to the conclusion that without such a complete theoretical basis, one would never have reached such good performances.

12.11 Development of an Ambulatory Instrument

The next step of this study was the development of an ambulatory instrument for the combined measurement of the micro– and macrotexture of real road surfaces [64] [65] [66].

In the right column of TABLE 12.1, one presents the requirements to be fulfilled by the instrument regarding macrotexture: the profiles must cover an horizontal length of 500 mm, while presenting a vertical resolution of 10 μm at least. At the moment, it is not possible to use structured lighting to develop a sensor showing such performances at a reasonable working distance ($\approx$ 10 cm).

The solution we opted for consists in moving a spot sensor—measuring the height of one point at a time—along a definite path. In order to take into account the possible anisotropies of the road, we opted for a 500-mm-circumference circular path. By associating the height of each measured point with the sensor position at the corresponding moment, we can reconstitute the macroprofile with a high accuracy.

Industry proposes a large variety of laser rangefinders offering a satisfactory resolution. Such a sensor, mounted on a high-precision rotation stage, is used. The microtexture determination is of course performed by the device presented in this chapter. It is mounted on a vertical translation stage interdependent with, and at a known distance of the macrotexture sensor.

As said at the beginning of the chapter, the combined measurement of both the micro– and macrotexture is necessary to obtain pertinent *skid resistance* estimations. However, macrotexture analyzes show that the vertical range of road profiles can go up to 20 mm, with generally steep variations. It is thus impossible for a vehicle tire to be simultaneously in contact with all the local hollows and peaks of the road. Consequently, microtexture analyzes can be executed on judiciously chosen macrotexture peaks only.

Those points are identified by mean of a method derived from the physics of the road/tire contact: the implemented algorithm firstly determines the local peaks likely to be in contact with the tire (this requires the choice of a pertinent contact depth) and then randomly selects a certain amount of them, where microtexture analyzes will be performed. For each point, the device must position itself correctly in the horizontal plane (peak selection with the rotation stage) and in the vertical plane (focusing with the translation stage, seen the limited depth of field of the microtexture sensor).

Fig. 12.10 shows a 3-D representation of the prototype, which is also pictured on Fig. 12.11. TABLE 12.2 summarizes the performances achieved by the instrument. For further technical explanations, see [64].

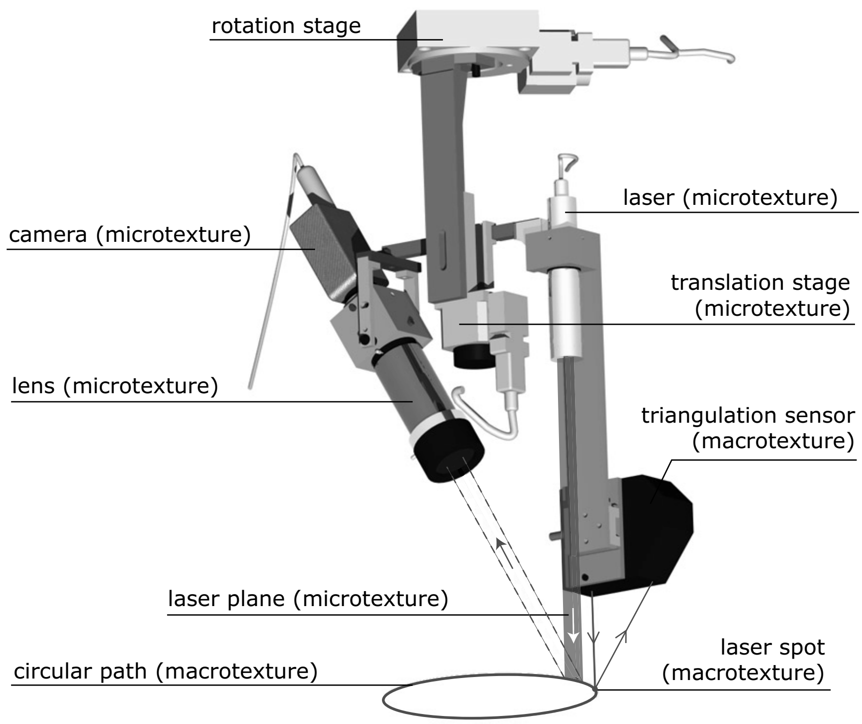

Fig. 12.10. 3-D representation of the prototype.

Table 12.2. Performances Achieved by our Instrument

quantity	microtexture	macrotexture
texture wavelengths	50–500 μm	0.5–200 mm
horizontal length of the profile	2 mm	500 mm
horizontal sampling interval	3.5 ± 0.05 μm	200 ± 1 μm
vertical range	4 mm	30 mm
vertical resolution	1 μm	6μm
vertical accuracy	10 μm	30 μm

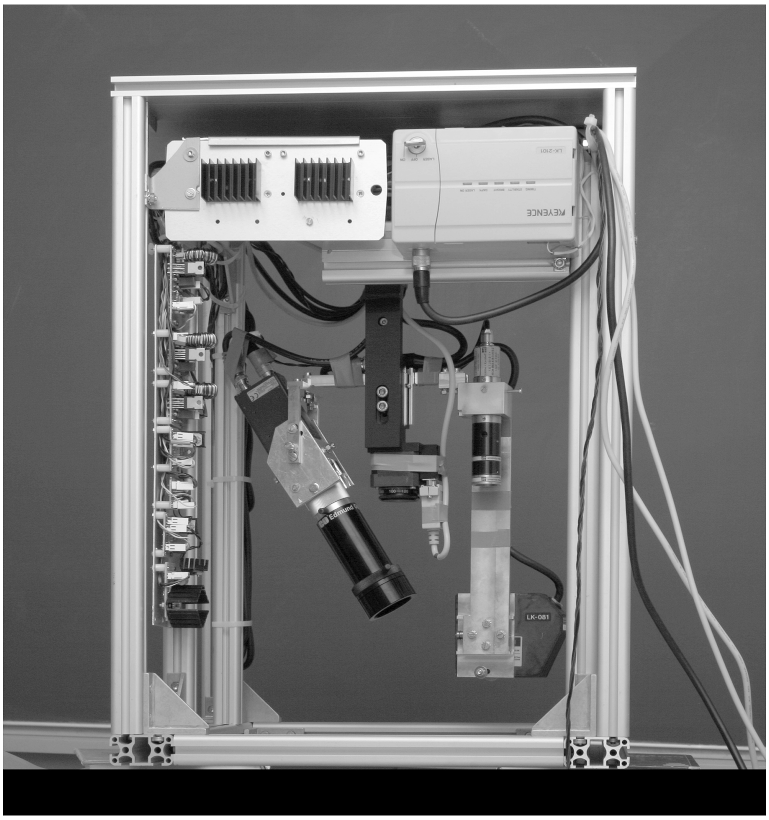

Fig. 12.11. Photograph of the prototype.

12.12 Illustration on a Road Surface

As an illustration of the device, we show in this section the results obtained on a real road, composed of bituminous aggregates (see picture on Fig. 12.12).

Fig. 12.12. Photograph of the road, composed of bituminous aggregates.

The macroprofile is presented on Fig. 12.13, together with the ten points selected for the microtexture analysis (squares). One of the microprofiles is shown on Fig. 12.14.

12.13 Conclusions

The feasibility of a new method for the determination of the road microtexture, based on laser triangulation under structured lighting, was studied.

The calibration procedure performed with our pre-prototype on a piezoelectric actuator, and the validation of the method on calibrated profiles make us claim an accuracy of the order of 10 μm on the vertical amplitude.

An ambulatory instrument for the combined measurement of both the micro– and macrotexture of road surfaces was developed. Its performances are in agreement with those of the Belgian Road Research Center, summarized on Table 12.1. We illustrate its functioning of a road composed of bituminous aggregates.

The next step—beyond the scope of this thesis—will be the study of the correlation between the *skid resistance* of the road surface obtained by the pendulum test method [57] and its micro– and macrotexture.

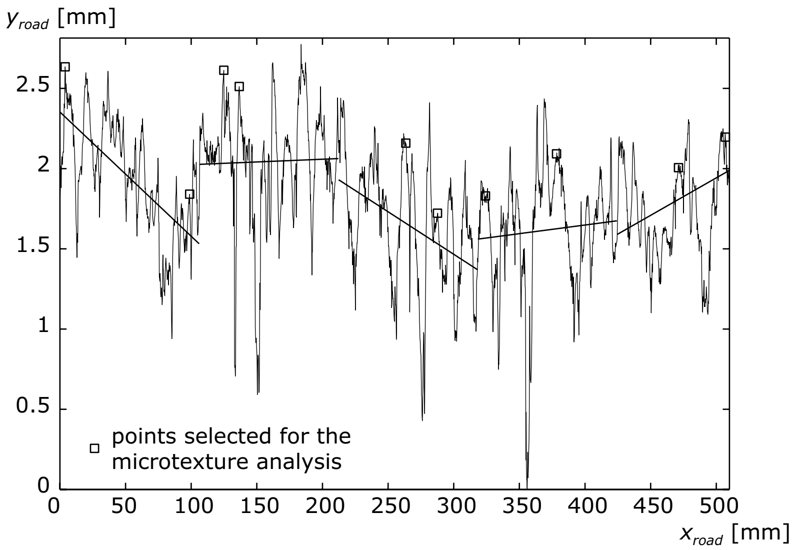

Fig. 12.13. Macrotexture analysis, showing an amplitude range of approximatively 3 mm.

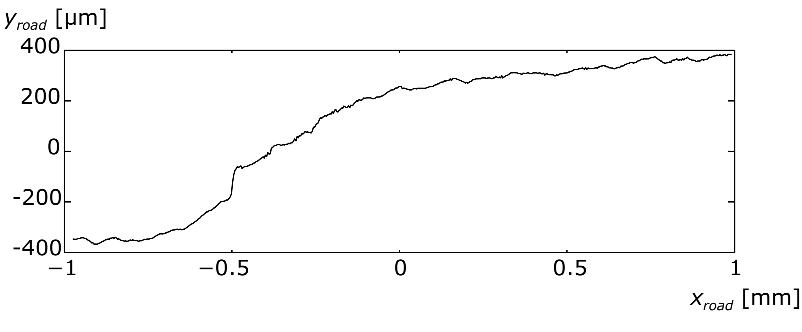

Fig. 12.14. Microtexture analysis on one macrotexture peak. The graph shows an amplitude range of approximatively 800 μm.